

Ternary Na-P-H superconductor under high pressureWeiguo Sun,^{1,2} Bole Chen,³ Xiaofeng Li,¹ Feng Peng,^{1,*} Andreas Hermann,⁴ and Cheng Lu^{2,†}¹*College of Physics and Electronic Information, Luoyang Normal University, Luoyang 471022, China*²*School of Mathematics and Physics, China University of Geosciences (Wuhan), Wuhan 430074, China*³*School of Science, Chongqing University of Posts and Telecommunications, Chongqing 400065, China*⁴*Centre for Science at Extreme Conditions and SUPA, School of Physics and Astronomy, University of Edinburgh, Edinburgh EH9 3FD, United Kingdom*

(Received 10 April 2023; accepted 1 June 2023; published 14 June 2023)

Most of the H-rich superconductors have so far been discovered to be clathrate structures. Several clathrate hydrides, including H_3S , LaH_{10} , and CaH_6 , were predicted to be excellent superconductors through structural searches and were later confirmed through experimental synthesis. Here, we conduct extensive crystal structure searches and first-principles calculations for ternary Na-P-H hydrides under high pressure. Two stoichiometries of NaPH_6 and NaPH_8 in ternary Na-P-H hydrides are found to be stable under 200 GPa. The $P\bar{6}m2$ phase of the NaPH_6 hydride is identified as a novel ternary layered H-rich superconductor, exhibiting a high critical temperature T_c of 112.2 K under 200 GPa. Our calculations indicate that the high T_c of the NaPH_6 hydride under high pressure is attributed to the high density of hydrogen s states present at the Fermi level. Furthermore, a metastable $Pm\bar{3}$ phase of the clathrate NaPH_6 hydride is uncovered under 350 GPa and displays an exceptional T_c of 201.4 K. These results suggest that ternary alkali metal Na-based hydrides hold promise as high- T_c superconductors under high pressure and offer critical insights into the design and synthesis of novel category high-temperature superconductors.

DOI: [10.1103/PhysRevB.107.214511](https://doi.org/10.1103/PhysRevB.107.214511)**I. INTRODUCTION**

Strong electron-phonon coupling (EPC) and high-frequency phonon vibrations make metallic hydrogen a promising high-temperature superconductor [1–3]. However, the metallization pressure required for dense hydrogen exceeds 450 GPa [4,5], which is still a challenge for current hydrostatic pressure experiments. A flexible strategy, “precompression” of hydrogen in hydrogen-dominant hydrides, proposed by Ashcroft [6] in 2004, can produce metallic hydrogen at relatively low pressure conditions. Several high-temperature superconductors in hydrides at high pressure were discovered with this powerful strategy, such as conventional sulfur hydrides (H_3S) [7,8], lanthanum hydrides (LaH_{10}) [9,10], and calcium hydrides (CaH_6), which were theoretically predicated to be metallic and subsequently confirmed by high-pressure experiments. These high- T_c superconductors exhibit high T_c values of 203 K at 150 GPa [11], 250 K at 170 GPa [12,13], and 215 K at 172 GPa [14], respectively. Therefore, the compressed hydrides experience metallization at much lower pressures than metallic hydrogen.

Since then, a series of surprising metallic hydrides with rather high T_c were searched for using extensive theoretical predictions [15–22]. The sodalitelike clathrate MgH_6 is predicted with T_c higher than 200 K [21,22] under high pressure [14,15]. In a recent review Semenok *et al.* reported the detailed

structure, electronic properties, and maximum T_c values for alkali metal and transition metal based binary hydrides [19], which offer active guidance for future synthesis of binary hydrides. As for rare-earth (RE) hydrides, Peng *et al.* conducted a symmetrical study for entire lanthanide series of elements, and the T_c values of the energetically stable YH_{10} and LaH_{10} hydrides are 303 and 288 K at high pressure [10]. We have also explored high- T_c superconductivity in H-rich RE hydrides and identified the “second island” of high- T_c superconductors in late Yb/Lu polyhydrides [23]. Moreover, yttrium hydrides with high symmetrized H cages in corresponding crystal structures are also potential superconductors. Some stable and metastable yttrium hydrides, such as YH_3 , YH_6 , and YH_9 , were successfully predicted and confirmed by the later experiments [24–27].

Recent reports [28,29] identified ternary hydrides that undergo metallization at moderate pressures while exhibiting high T_c values, potentially even at room temperature. Sun *et al.* discovered the metastable $\text{Li}_2\text{MgH}_{16}$ [30] ternary hydride with a remarkably high T_c value of ~ 473 K at 250 GPa. The doped Li atoms in $\text{Li}_2\text{MgH}_{16}$ provide extra electrons to dissociate the H_2 molecules, which greatly improves the strong EPC and causes the high- T_c superconductivity. Alkali metals (Li) and alkaline earth metals (Mg, Ca) can donate electrons [31–36] to enhance the T_c of hydrides. For example, phosphorus hydrides are metastable phases corresponding to elemental phosphorus and hydrogen [35–37]. The free-electron metal Li ([He] $2s^1$) doped metastable P-H binary hydrides, such as $\text{LiP}_2\text{H}_{14}$ (169 K at 230 GPa) [38] and LiPH_6 (167 K at 200 GPa) [39], can produce stable high- T_c

*fpeng@calypso.cn

†lucheng@calypso.cn

superconductors. By contrast, the atomic radius of sodium is about 1.8 Å, which is larger than that of lithium. The metallized pressures of sodium-based hydrides are, in principle, lower than those of lithium hydrides [40,41]. For instance, Na₃FeH₇ and Na₃CoH₆ hydrides exhibit low synthesis pressures of about 10 GPa [42], and Na₂SiH₆ hydrides are known to form several hypervalent compounds which exhibit superionicity at relatively low pressure.

In this work, we conduct a systematic study of sodium metal doped phosphorus hydrides, producing stabilized NaPH_{*n*} (*n* = 3–8) ternary hydrides under high pressure. The energetic, structural, and electronic properties of the stable H-rich NaPH₆ and NaPH₈ hydrides indicate that NaPH₆ are energetic and dynamic stable at 200 GPa. Furthermore, the hexagonal layered *P* $\bar{6}m2$ phase of NaPH₆ is an excellent superconductor with a high *T_c* of 112.2 K at 200 GPa, while the cubic clathrate *Pm* $\bar{3}$ phase of NaPH₆ exhibits a *T_c* value of 201.4 K at 350 GPa. The *Pm* phase of NaPH₈ is metallic at 200 GPa with *T_c* of 55.9 K, suggesting that H-rich NaPH₆ and NaPH₈ hydrides are high-*T_c* superconductors.

II. COMPUTATIONAL DETAILS

The candidate structures of ternary Na-P-H hydrides are predicted using the CALYPSO code [43–45]. We perform variable-composition crystal structure searches for NaPH_{*n*} (*n* = 3–8) ranging from 1 to 4 f.u./cell at 100, 200, 300, and 400 GPa. The total energy and electronic properties are calculated by using the Vienna Ab initio Simulation Package (VASP) [46] with the Perdew-Burke-Ernzerhof [47] exchange-correlation functional. Projector augmented wave (PAW) potentials with the valence electrons 3s¹ for Na, 3s²3p³ for P, and 1s¹ for H are adopted [48]. Valid PAW pseudopotentials under high pressure have been verified by various works [10,23,49]. For Na-P-H hydrides, the detailed core radii from the pseudopotentials and the interatomic distances (see the Supplemental Material [50]) indicate that the PAW pseudopotential can lead to solid and valid results in high-pressure calculations. To ensure the convergence of force and energy, we set the corresponding plane wave cutoff energy to 800 eV and Brillouin zone samplings to 0.20 Å⁻¹. The dynamical stability of the predicated ternary Na-P-H hydrides is calculated using the PHONOPY code [51] by using density functional perturbation theory. The EPC and superconducting critical temperature *T_c* are calculated using the QUANTUM ESPRESSO package [52]. Ultrasoft pseudopotentials for Na, P, and H atoms are chosen with a kinetic energy cutoff of 80 Ry. To get the EPC parameter λ , the Brillouin zone is sampled by a very dense 24 × 24 × 24 mesh for *k* points and a 6 × 6 × 6 *q*-point mesh (convergence tests are shown in Fig. S1). *T_c* are estimated using the Allen-Dynes modified McMillan equation [53],

$$T_c = \frac{\omega_{\log}}{1.2} \exp\left(\frac{-1.04(1 + \lambda)}{\lambda - \mu^*(1 + 0.62\lambda)}\right), \quad (1)$$

which considers the strong coupling and shape correction multipliers of *f*₁ and *f*₂:

$$f_1 = \left[1 + \left(\frac{\lambda}{2.46(1 + 3.8\mu^*)}\right)^{\frac{3}{2}}\right]^{\frac{1}{3}}, \quad (2)$$

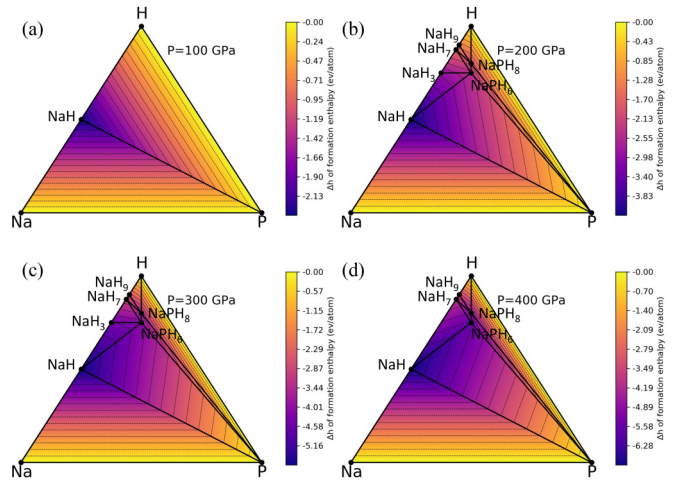


FIG. 1. (a)–(d) The 3D convex hulls constructed based on the formation enthalpies related to the elemental Na, P, and H at 100, 200, 300, and 400 GPa, respectively; the solid dotted (NaPH₆ and NaPH₈) represent the energetically stable structures.

$$f_2 = 1 + \frac{(\frac{\bar{\omega}}{\omega_{\log}} - 1)\lambda^2}{\lambda^2 + [1.82(1 + 6.3\mu^*)\frac{\bar{\omega}}{\omega_{\log}}]^2}, \quad (3)$$

$$T_c = f_1 f_2 \frac{\omega_{\log}}{1.2} \exp\left(\frac{-1.04(1 + \lambda)}{\lambda - \mu^*(1 + 0.62\lambda)}\right). \quad (4)$$

Coulomb pseudopotentials $\mu^* = 0.10$ and 0.13 are taken in our calculation. The EPC constants of λ and ω_{\log} are calculated as

$$\lambda = 2 \int_0^\infty \frac{\alpha^2 F(\omega)}{\omega} d\omega, \quad (5)$$

$$\omega_{\log} = \exp\left[\frac{\lambda}{2} \int_0^\infty \frac{d\omega}{\omega} \alpha^2 F(\omega) \ln(\omega)\right]. \quad (6)$$

III. RESULTS AND DISCUSSION

We have explored the energetically stable structures of NaPH_{*n*} (*n* = 3–8) hydrides at pressures ranging from 100 to 400 GPa. Clearly, the ternary stoichiometries of NaPH₆ and NaPH₈ hydrides occur in three-dimensional (3D) convex hulls, as depicted in Fig. 1. Based on the formation enthalpies relative to the elemental Na, P, and H atoms, we have identified energetically stable binary NaH, NaH₃, NaH₇, and NaH₉ hydrides and ternary NaPH₆ and NaPH₈ hydrides. Figures 1(a)–1(d) show that the ternary NaPH₆ and NaPH₈ hydrides remain stable up to 200 GPa. Additionally, in Figs. S2(a)–S2(c) in the Supplemental Material [50], we present the 3D convex hulls of NaPH₆ and NaPH₈ hydrides with respect to the stabilized binary NaH hydride and elemental P and H atoms. The enthalpy difference curves for NaPH₆ with respect to the *R* $\bar{3}m$ phase as a function of pressure are shown in Fig. S3(a), which suggests that the hexagonal layered *P* $\bar{6}m2$ phase of NaPH₆ remains stable over the pressure range of 200 to 400 GPa. Our structure predictions have also uncovered two metastable *R* $\bar{3}m$ and *Pm* $\bar{3}$ phases of NaPH₆. The monoclinic *Pm* phase of NaPH₈ is identified as the ground state structure at high pressure from 200 to

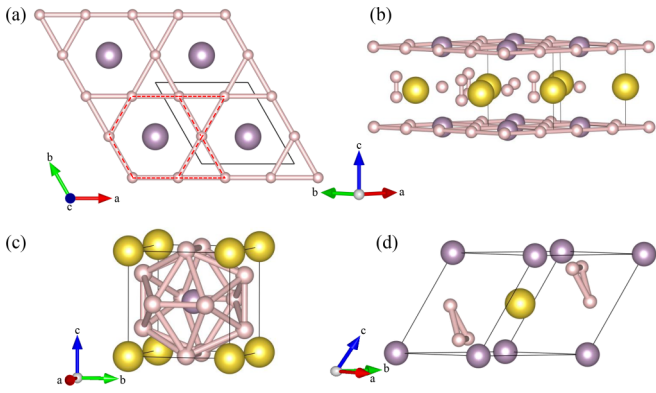


FIG. 2. Crystal structures for NaPH_6 : (a) and (b) a supercell of $P\bar{6}m2$ NaPH_6 at 200 GPa in different views, with the kagome lattice formed by H atoms in the H-P layer, (c) the $Pm\bar{3}$ structure at 350 GPa, and (d) the $R\bar{3}m$ structure at 200 GPa. The sodium atoms are yellow, the phosphorus atoms are purple, and the hydrogen atoms are pink.

350 GPa, as illustrated in Fig. S3(b). Figures S4–S6 display the phonon dispersion curves of the $P\bar{6}m2$, $R\bar{3}m$, and $Pm\bar{3}$ phases of NaPH_6 , indicating that the $P\bar{6}m2$ phase is thermodynamically stable within a pressure range of 150 to 400 GPa.

Detailed crystal structures of NaPH_6 hydrides for selected pressures are displayed in Figs. 2 and S7. The corresponding structure parameters are summarized in Table S1. Typically, H-rich clathrate structures are observed in binary and ternary H-rich superconductors. However, the most stable structure of the NaPH_6 hydride at 200 GPa is a layered $P\bar{6}m2$ phase, which consists of H-P and Na-H layers, as depicted in Figs. 2(a) and 2(b). The H_2 units are bonded with the P-H and Na-H layers; the corresponding H-H distance is about 0.774 Å. The H atoms in the P-H layers form a kagome lattice [in Fig. 2(a)], while the P atoms are centered within each kagome framework [54]. Additionally, a H-rich clathrate structure of the NaPH_6 hydride with $Pm\bar{3}$ symmetry is identified. The cubic $Pm\bar{3}$ phase of the NaPH_6 hydride is metallic and stable at 350 GPa, as depicted in Fig. 2(c). The H_{12} cages are surrounded by P atoms, which is similar to the previously reported LiPH_6 hydride [39]. Another metastable phase of NaPH_6 is observed in the structural searches at 200 GPa and is a trigonal $R\bar{3}m$ structure, as shown in Fig. 2(d), where the H atoms are arranged in triangular H_3 units. Na atoms are located at the eight corners of the lattice, while the P atoms are situated in the body-centered lattice. Although the trigonal $R\bar{3}m$ phase and cubic $Pm\bar{3}$ phase of NaPH_6 possess formation enthalpies that are approximately 0.044 and 0.182 eV/atom higher, respectively, than that of the ground state $P\bar{6}m2$ phase at 200 GPa, they are still regarded as metastable phases due to their mechanical and thermodynamic instability.

In Fig. 3(a), we present the electronic band structure and density of states (DOS) for the most stable $P\bar{6}m2$ phase of NaPH_6 at 200 GPa. The flat electronic bands crossing the Fermi level indicate the metallic character of the $P\bar{6}m2$ phase. The H s states contribute to half of the total DOS at the Fermi level, and their high values suggest that the $P\bar{6}m2$ phase of

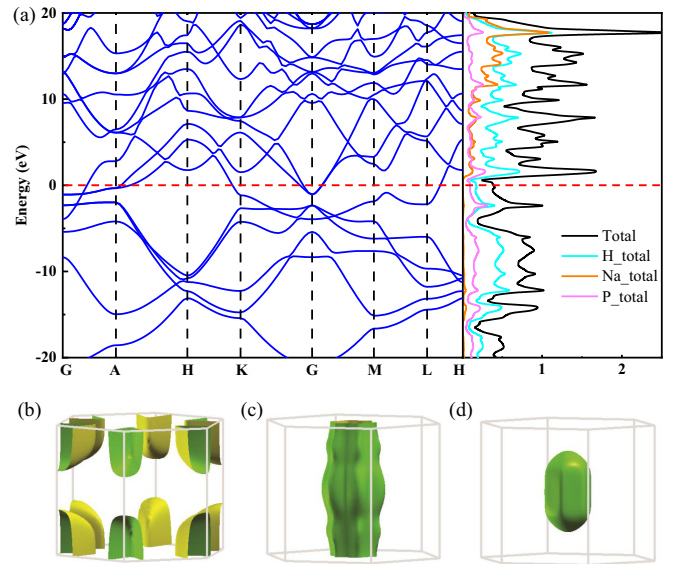


FIG. 3. (a) Calculated electronic band structures and density of states of $P\bar{6}m2$ NaPH_6 and (b)–(d) the Fermi surface sheets of the $P\bar{6}m2$ NaPH_6 structure at 350 GPa.

NaPH_6 is a potential high- T_c superconductor [23]. The Fermi surface of the $P\bar{6}m2$ phase, shown in Figs. 3(b)–3(d), reveals that the electron packages are located around the Γ point. Furthermore, we display the detailed DOS and Fermi surface sheets for the metastable $R\bar{3}m$ and $Pm\bar{3}$ phases at 350 GPa in Fig. S10, which shows that both the $R\bar{3}m$ and $Pm\bar{3}$ phases of NaPH_6 are metallic with a relatively large number of H s states at the Fermi level.

Motivated by the metallic properties of the NaPH_6 hydride, we have calculated the EPC parameters for both stable and metastable hydrides at high pressure. The electronic density of states at the Fermi level N_{E_f} , the detailed EPC parameter λ , the logarithmic average phonon frequency ω_{log} , and the superconductivity T_c are summarized in Table I. The results indicate that the layered $P\bar{6}m2$ structure possesses a high T_c of 112.2 K ($\lambda = 1.313$) at 200 GPa and 93.4 K ($\lambda = 0.904$) at 350 GPa when $\mu^* = 0.10$. The layered $P\bar{6}m2$ phase represents a category of high- T_c hydrides that expands the range of known covalent and clathrate superhydrides [29]. Our calculations indicate that the EPC λ value for the $Pm\bar{3}$ phase of NaPH_6 is approximately 2.347. For EPC $\lambda > 1.5$, by considering the Allen-Dynes modified McMillan equation, the T_c superconductivity of the cubic $Pm\bar{3}$ phase of NaPH_6 is determined to be 201.4 K, which is higher than the T_c of approximately 167.3 K for the similar cubic $Pm\bar{3}$ phase of LiPH_6 [39]. Furthermore, the metastable trigonal $R\bar{3}m$ phase of NaPH_6 exhibits a T_c value of 95.9 K ($\lambda = 1.313$) at 350 GPa. The remarkable superconductivity observed in NaPH_6 suggests that Na atoms could provide electrons to increase the contribution of the DOS of atomic hydrogen around the Fermi level and could result in high T_c values. Based on the N_{E_f} values presented in Table I, it can be observed that high N_{E_f} values correspond to high T_c values, as evidenced by the $P\bar{6}m2$, $R\bar{3}m$, and $Pm\bar{3}$ phases of NaPH_6 exhibiting higher T_c values at selected

TABLE I. Predicted superconducting properties of ternary Na-P-H high-temperature superconducting polyhydrides at different pressures; T_c are estimated using the McMillan equation and the Allen-Dynes modified McMillan equation.

Hydrides	Space group	Pressure (GPa)	N_{Ef} [states/(Ry/f.u.)]	λ	ω_{\log} (K)	T_c (K)		$f_1 f_2 T_c$ (K)	
						$\mu^* = 0.10$	$\mu^* = 0.13$		
NaPH ₆	187 ($P\bar{6}m2$)	150	4.231	3.311	377.277	70.7	67.5	110.5	
	187 ($P\bar{6}m2$)	200	3.766	1.313	1128.264	112.2	100.8		
	187 ($P\bar{6}m2$)	300	3.677	0.984	1417.528	96.3	82.4		
	187 ($P\bar{6}m2$)	350	3.601	0.904	1581.039	93.4	78.2		
	187 ($P\bar{6}m2$)	400	3.596	0.883	1503.430	85.1	70.8		
	166 ($R\bar{3}m$)	200	2.652	1.289	854.109	83.2	74.6		
	166 ($R\bar{3}m$)	300	3.173	1.496	905.954	103.0	93.9		118.8
	166 ($R\bar{3}m$)	350	2.633	1.313	964.058	95.9	86.1		
	200 ($Pm\bar{3}$)	340	5.375	2.257	997.160	155.0	145.6		196.1
	200 ($Pm\bar{3}$)	350	5.393	2.347	1009.917	160.6	151.2		201.4
200 ($Pm\bar{3}$)	400	5.065	2.235	726.923	112.3	105.5	145.2		
NaPH ₈	6 (Pm)	200	2.748	1.467	500.387	55.9	50.8		
	6 (Pm)	300	1.701	0.670	1995.376	62.1	46.6		
	6 (Pm)	350	2.456	1.192	764.332	67.8	60.1		

pressures. For example, the $P\bar{6}m2$ phase displays a T_c of 112.2 K (with a N_{Ef} value of ~ 3.766), while the $Pm\bar{3}$ phase exhibits a T_c of 201.4 K (with a N_{Ef} value of ~ 5.393). Comparing the superconductivity trends with the cubic $Pm\bar{3}$ phase of LiPH₆, we can infer that the alkali metal Na can stabilize P-H hydrides at high pressure and enhance the EPC, leading to high- T_c superconductivity.

To further explore the superconductivity mechanism in diverse structures of NaPH₆ hydrides, we have calculated the phonon dispersion curves; phonon density of states projected on Na, P, and H atoms; and THE Eliashberg spectral

function $\alpha^2 F(\omega)$ together with the electron-phonon integral $\lambda(\omega)$ at 350 GPa, as displayed in Fig. 4. The phonon modes for the layered $P\bar{6}m2$ phase [Fig. 4(a)] exhibit two distinct frequency ranges: Na and P atoms contribute minimally to the overall EPC λ due to their substantial atomic masses in the low-frequency range (0–750 cm^{-1}). Meanwhile, the high-frequency region ($>750 \text{ cm}^{-1}$) is predominantly associated with atomic H atom vibrations and H₂ molecules, contributing significantly to the total EPC λ (up to 67%), similar to H-dominated binary high- T_c superconductors such as H₃S [7,11] and lanthanide hydrides [10,12,13]. In Fig. 4(b), the

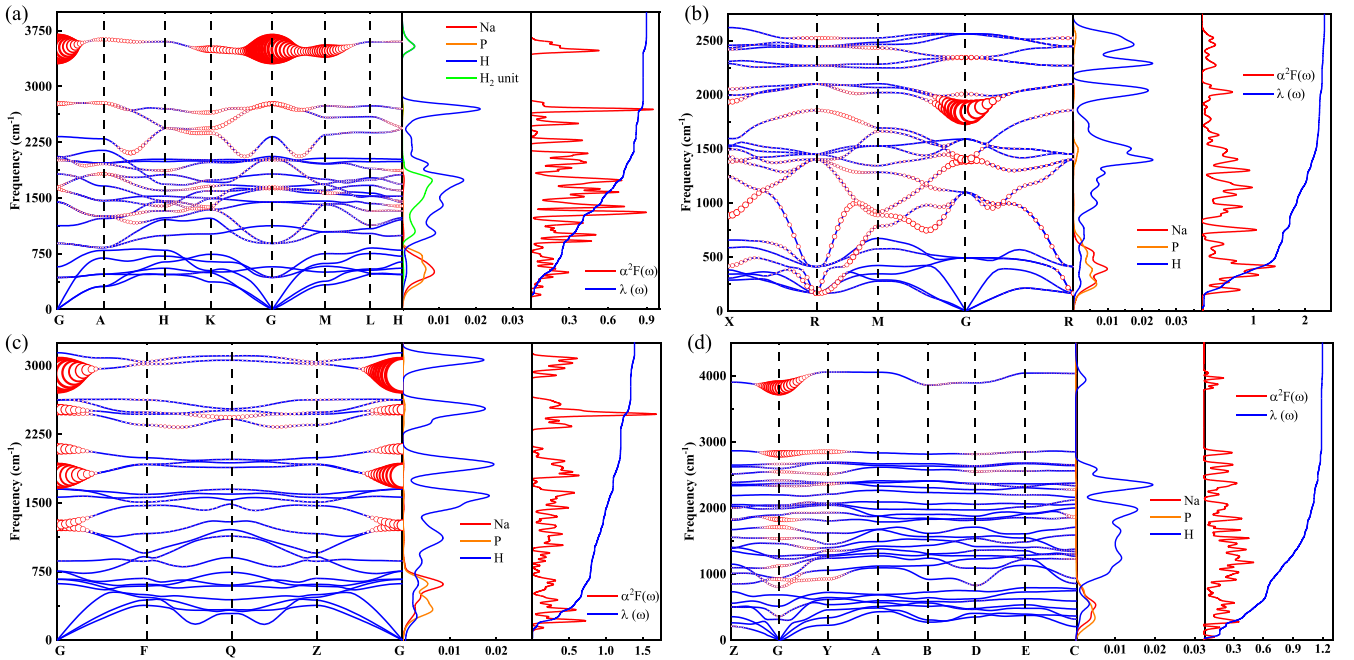


FIG. 4. Phonon dispersion curves (the radius of the red circle is parallel to phonon linewidths); phonon density of states projected on Na, P, and H atoms; and the Eliashberg spectral function $\alpha^2 F(\omega)$ together with the electron-phonon integral $\lambda(\omega)$ at 350 GPa for (a) the $P\bar{6}m2$ phase of NaPH₆, (b) the $Pm\bar{3}$ phase of NaPH₆, (c) the $R\bar{3}m$ phase of NaPH₆, and (d) the Pm phase of NaPH₈.

clathrate $Pm\bar{3}$ phase of NaPH_6 exhibits a compelling soft phonon mode in the middle frequency ($250\text{--}1500\text{ cm}^{-1}$) at the R point. The radius of the red circle on the phonon dispersion curve represents the strength of the EPC λ , indicating that considerable phonon linewidths mainly originate from the H-H vibration soft phonon modes around the R and Γ points for $Pm\bar{3}$ NaPH_6 at 350 GPa. The phonon modes in the low-frequency region ($<750\text{ cm}^{-1}$) are predominantly related to the Na/P atoms and a portion of the H-H soft phonon, resulting in 70% of the total EPC λ , while the atomic H-H vibration phonon modes dominate the high frequency $>750\text{ cm}^{-1}$ with 30% of the EPC λ [see Fig. 4(b)]. Interestingly, the vibrational range of hydrogen atoms in the trigonal $R\bar{3}m$ phase of NaPH_6 is different from those of layered and cubic structures, which appear in the entire vibration frequency region [see Fig. 4(c)]. For the $R\bar{3}m$ phase of the NaPH_6 hydride, H atoms combined with Na and P atoms contribute about 45% of the total EPC λ in the low-frequency range. Hydrogen plays the dominating role in strong EPC, leading to high- T_c ternary atomic hydride superconductors. Overall, among the three phases of NaPH_6 hydride superconductors, the metastable $Pm\bar{3}$ phase with atomic hydrogen possesses the highest T_c value of approximately 201.4 K at 350 GPa, attributed to the Na/P vibrations in the low-frequency region contributing 70% of the total EPC λ . Meanwhile, the layered $P\bar{6}m2$ ground state and trigonal $R\bar{3}m$ metastable for NaPH_6 display T_c values of around 93.4 and 95.9 K at 350 GPa, respectively.

We next calculate the projected crystal orbital Hamiltonian population [55–57] to evaluate the chemical bonding in Na-P-H hydrides, which can provide critical insights into the relationships between superconductivity and structure among the different phases of NaPH_6 . Figure 5(a) reveals strong H-H bonding in the layered $P\bar{6}m2$ phase of NaPH_6 , evidenced by the prominent features of occupied antibonding states near the Fermi level. The substantial antibonding states of H-H bonding, including the H-H bonding in molecular H_2 , agree with the dominant contribution of 67% to the total EPC λ in the $P\bar{6}m2$ phase of NaPH_6 at 350 GPa. It is noteworthy that the Na-H and P-H bonding states are qualitatively similar in the cubic $Pm\bar{3}$ and trigonal $R\bar{3}m$ phases of NaPH_6 [Figs. 5(b) and 5(c)], with occupied bonding states below and antibonding states above the Fermi level, respectively. Moreover, in the cubic $Pm\bar{3}$ phase of NaPH_6 , the H atoms contribute to strong H-H bonding states near the Fermi level [Fig. 5(c)], indicating the highest T_c values. Table S1 presents the detailed Bader charges of Na, P, and H atoms of NaPH_6 hydrides at 350 GPa, indicating the number of electrons transferred from Na/P to H atoms. For the three phases of NaPH_6 hydrides, the partial charges transferred in the layered $P\bar{6}m2$ phase are $-0.61e$ and $-0.62e$ for Na and P, respectively. Similar values are observed in the cubic $Pm\bar{3}$ ($-0.47e$ for Na and $-1.29e$ for P) and trigonal $R\bar{3}m$ ($-0.57e$ for Na and $-2.53e$ for P) phases of NaPH_6 at 350 GPa, with H atoms accepting all electrons from the Na and P atoms. The formation of metallic H-H bonds by charge transfer from Na and P atoms induces the high-frequency vibration and causes the high- T_c superconductivity of NaPH_6 . For the ground state layered $P\bar{6}m2$ phase of NaPH_6 , the $2h$ and $2c$ sites of H atoms represent the H_2 molecules, corresponding to a nearly negligible electron transfer of $0.03e$. The

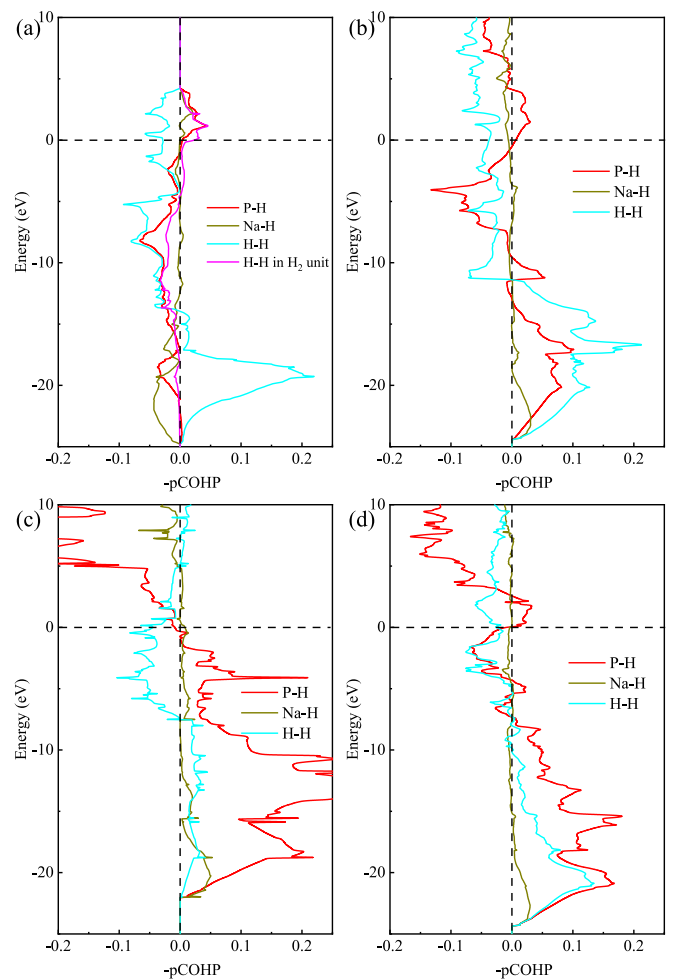


FIG. 5. Projected crystal orbital Hamiltonian population (pCOHP) of the predicted compounds: (a) the $P\bar{6}m2$ phase of NaPH_6 , (b) the $R\bar{3}m$ phase of NaPH_6 , (c) the $Pm\bar{3}$ phase of NaPH_6 , and (d) the Pm phase of NaPH_8 at 350 GPa.

significant degree of electron transfer from Na/P atoms to H atoms in the ternary $P\bar{6}m2$, $R\bar{3}m$ and $Pm\bar{3}$ hydrides promotes the formation of Na-H and P-H bonds, as well as high-frequency hydrogen vibrations, which is consistent with the above EPC calculations.

In fact, we have found another stable stoichiometry of NaPH_8 in ternary Na-P-H hydrides at 200 GPa. It is also a layered structure with Pm symmetry, as shown in Fig. S7(c), and is composed of Na- H_2 -H and P-H layers. The H-H distance within the H_2 unit is approximately 0.742 \AA . As shown in Fig. S9(b), the calculated band structures and DOS indicate the Pm phase of NaPH_8 possesses a limited metallic character. The corresponding EPC calculations reveal that the Pm phase of NaPH_8 shows a T_c value of 67.8 K ($\lambda \sim 1.192$), which is lower than that of the layered $P\bar{6}m2$ phase of NaPH_6 ($T_c \sim 93.4\text{ K}$) at 350 GPa. For the Pm phase of NaPH_8 , the analogous vibration phonon modes are also presented in Fig. 4(d). The soft phonon modes around the Γ point indicate the H atom vibrations effectively enhance the EPC, and H atoms dominate the high-frequency regions ($>750\text{ cm}^{-1}$) with 42% of the total λ .

IV. CONCLUSIONS

In summary, we have explored the crystal structures and superconductivity of H-rich Na-P-H ternary hydrides at 100–400 GPa by using structure prediction methods and first-principles calculations. We have discovered two stable stoichiometries of NaPH₆ and NaPH₈ in ternary Na-P-H hydrides at 200 GPa. The $P\bar{6}m2$ phase of NaPH₆ was verified as a ternary layered H-rich superconductor with a high T_c value of 112.2 K at 200 GPa. Interestingly, the metastable clathrate $Pm\bar{3}$ phase of NaPH₆ was identified with a substantial T_c value of 201.4 K at 350 GPa. Our calculations demonstrate that the high T_c of NaPH₆ at high pressure is due to the high density of H s states at the Fermi level, and H atoms contribute to strong EPC interactions in ternary sodium

phosphorus hydrides. These findings enrich the understanding of alkali metal phosphorus hydrides at high pressure and provide vital perspectives for further exploration of innovative classes of high-temperature superconductors.

ACKNOWLEDGMENTS

This work was supported by the National Natural Science Foundation of China (Grants No. 12174352, No. 12111530103, and No. 12174170). W.S. acknowledges funding from the Key Research Project in University of Henan Province under Grant No. 22A140025 and the Natural Science Foundation of Henan Province under Grant No. 232300420352.

-
- [1] P. Loubeyre, F. Occelli, and P. Dumas, *Nature (London)* **577**, 631 (2020).
- [2] P. Loubeyre, F. Occelli, and R. LeToullec, *Nature (London)* **416**, 613 (2002).
- [3] N. W. Ashcroft, *Phys. Rev. Lett.* **21**, 1748 (1968).
- [4] J. M. McMahon and D. M. Ceperley, *Phys. Rev. B* **84**, 144515 (2011).
- [5] P. Cudazzo, G. Profeta, A. Sanna, A. Floris, A. Continenza, S. Massidda, and E. K. U. Gross, *Phys. Rev. Lett.* **100**, 257001 (2008).
- [6] N. W. Ashcroft, *Phys. Rev. Lett.* **92**, 187002 (2004).
- [7] D. Duan, Y. Liu, F. Tian, D. Li, X. Huang, Z. Zhao, H. Yu, B. Liu, W. Tian, and T. Cui, *Sci. Rep.* **4**, 6968 (2014).
- [8] Y. Li, J. Hao, H. Liu, Y. Li, and Y. Ma, *J. Chem. Phys.* **140**, 174712 (2014).
- [9] H. Liu, I. I. Naumov, R. Hoffmann, N. W. Ashcroft, and R. J. Hemley, *Proc. Natl. Acad. Sci. USA* **114**, 6990 (2017).
- [10] F. Peng, Y. Sun, C. J. Pickard, R. J. Needs, Q. Wu, and Y. Ma, *Phys. Rev. Lett.* **119**, 107001 (2017).
- [11] A. P. Drozdov, M. I. Erements, I. A. Troyan, V. Ksenofontov, and S. I. Shylin, *Nature (London)* **525**, 73 (2015).
- [12] A. P. Drozdov, P. P. Kong, V. S. Minkov, S. P. Besedin, M. A. Kuzovnikov, S. Mozaffari, L. Balicas, F. F. Balakirev, D. E. Graf, V. B. Prakapenka *et al.*, *Nature (London)* **569**, 528 (2019).
- [13] M. Somayazulu, M. Ahart, A. K. Mishra, Z. M. Geballe, M. Baldini, Y. Meng, V. V. Struzhkin, and R. J. Hemley, *Phys. Rev. Lett.* **122**, 027001 (2019).
- [14] L. Ma, K. Wang, Y. Xie, X. Yang, Y. Wang, M. Zhou, H. Liu, X. Yu, Y. Zhao, H. Wang, G. Liu, and Y. Ma, *Phys. Rev. Lett.* **128**, 167001 (2022).
- [15] Z. Li, X. He, C. Zhang, X. Wang, S. Zhang, Y. Jia, S. Feng, K. Lu, J. Zhao, J. Zhang *et al.*, *Nat. Commun.* **13**, 2863 (2022).
- [16] D. F. Duan, Y. X. Liu, Y. B. Ma, Z. Shao, B. B. Liu, and T. Cui, *Natl. Sci. Rev.* **4**, 121 (2017).
- [17] E. Zurek and T. G. Bi, *J. Chem. Phys.* **150**, 050901 (2019).
- [18] J. A. Flores-Livas, L. Boeri, A. Sanna, G. Profeta, R. Arita, and M. Erements, *Phys. Rep.* **856**, 1 (2020).
- [19] D. V. Semenok, I. A. Kruglov, I. A. Savkin, A. G. Kvashnin, and A. R. Oganov, *Curr. Opin. Solid State Mater. Sci.* **24**, 100808 (2020).
- [20] D. C. Lonie, J. Hooper, B. Altintas, and E. Zurek, *Phys. Rev. B* **87**, 054107 (2013).
- [21] H. Wang, J. S. Tse, K. Tanaka, T. Iitaka, and Y. Ma, *Proc. Natl. Acad. Sci. USA* **109**, 6463 (2012).
- [22] X. Feng, J. Zhang, G. Gao, H. Liu, and H. Wang, *RSC Adv.* **5**, 59292 (2015).
- [23] W. Sun, X. Kuang, H. D. J. Keen, C. Lu, and A. Hermann, *Phys. Rev. B* **102**, 144524 (2020).
- [24] I. A. Troyan, D. V. Semenok, A. G. Kvashnin, A. V. Sadakov, O. A. Sobolevskiy, V. M. Pudalov, A. G. Ivanova, V. B. Prakapenka, E. Greenberg, A. G. Gavriliuk *et al.*, *Adv. Mater.* **33**, 2006832 (2021).
- [25] J. Purans, A. P. Menushenkov, S. P. Besedin, A. A. Ivanov, V. S. Minkov, I. Pudza, A. Kuzmin, K. V. Klementiev, S. Pascarelli, O. Mathon *et al.*, *Nat. Commun.* **12**, 1765 (2021).
- [26] E. Snider, N. Dasenbrock-Gammon, R. McBride, X. Wang, N. Meyers, K. V. Lawler, E. Zurek, A. Salamat, and R. P. Dias, *Phys. Rev. Lett.* **126**, 117003 (2021).
- [27] Y. Li, J. Hao, H. Liu, J. S. Tse, Y. Wang, and Y. Ma, *Sci. Rep.* **5**, 9948 (2015).
- [28] X. Zhang, Y. Zhao, and G. Yang, *Wiley Interdiscip. Rev.: Comput. Mol. Sci.* **12**, e1582 (2021).
- [29] M. Du, W. Zhao, T. Cui, and D. Duan, *J. Phys.: Condens. Matter* **34**, 173001 (2022).
- [30] Y. Sun, J. Lv, Y. Xie, H. Liu, and Y. Ma, *Phys. Rev. Lett.* **123**, 097001 (2019).
- [31] X. Liang, A. Bergara, L. Wang, B. Wen, Z. Zhao, X.-F. Zhou, J. He, G. Gao, and Y. Tian, *Phys. Rev. B* **99**, 100505(R) (2019).
- [32] H. Xie, D. Duan, Z. Shao, H. Song, Y. Wang, X. Xiao, D. Li, F. Tian, B. Liu, and T. Cui, *J. Phys.: Condens. Matter* **31**, 245404 (2019).
- [33] Y. Yan, T. Bi, N. Geng, X. Wang, and E. Zurek, *J. Phys. Chem. Lett.* **11**, 9629 (2020).
- [34] D. Meng, M. Sakata, K. Shimizu, Y. Iijima, H. Saitoh, T. Sato, S. Takagi, and S. I. Orimo, *Phys. Rev. B* **99**, 024508 (2019).
- [35] J. A. Flores-Livas, M. Amsler, C. Heil, A. Sanna, L. Boeri, G. Profeta, C. Wolverton, S. Goedecker, and E. K. U. Gross, *Phys. Rev. B* **93**, 020508(R) (2016).
- [36] A. Shamp, T. Terpstra, T. Bi, Z. Falls, P. Avery, and E. Zurek, *J. Am. Chem. Soc.* **138**, 1884 (2016).
- [37] Y. Yuan, Y. Li, G. Fang, G. Liu, C. Pei, X. Li, H. Zheng, K. Yang, and L. Wang, *Natl. Sci. Rev.* **6**, 524 (2019).

- [38] X. Li, Y. Xie, Y. Sun, P. Huang, H. Liu, C. Chen, and Y. Ma, *J. Phys. Chem. Lett.* **11**, 935 (2020).
- [39] Z. Shao, D. Duan, Y. Ma, H. Yu, H. Song, H. Xie, D. Li, F. Tian, B. Liu, and T. Cui, *npj Comput. Mater.* **5**, 104 (2019).
- [40] C. Pépin, P. Loubeyre, F. Occelli, and P. Dumas, *Proc. Natl. Acad. Sci. USA* **112**, 7673 (2015).
- [41] Y. M. Chen, H. Y. Geng, X. Z. Yan, Y. Sun, Q. Wu, and X. R. Chen, *Inorg. Chem.* **56**, 3867 (2017).
- [42] K. Spektor, W. A. Crichton, S. Filippov, S. I. Simak, A. Fischer, and U. Häussermann, *Inorg. Chem.* **59**, 16467 (2020).
- [43] J. Lv, Y. Wang, L. Zhu, and Y. Ma, *J. Chem. Phys.* **137**, 084104 (2012).
- [44] Y. Wang, J. Lv, L. Zhu, and Y. Ma, *Phys. Rev. B* **82**, 094116 (2010).
- [45] B. Gao, P. Gao, S. Lu, J. Lv, Y. Wang, and Y. Ma, *Sci. Bull.* **64**, 301 (2019).
- [46] G. Kresse and J. Furthmüller, *Comput. Mater. Sci.* **6**, 15 (1996).
- [47] J. P. Perdew, K. Burke, and M. Ernzerhof, *Phys. Rev. Lett.* **77**, 3865 (1996).
- [48] G. Kresse and D. Joubert, *Phys. Rev. B* **59**, 1758 (1999).
- [49] A. R. Oganov, J. Chen, C. Gatti, Y. Ma, Y. Ma, C. W. Glass, Z. Liu, T. Yu, O. O. Kurakevych, and V. L. Solozhenko, *Nature (London)* **457**, 863 (2009).
- [50] See Supplemental Material at <http://link.aps.org/supplemental/10.1103/PhysRevB.107.214511> for the 3D convex hulls, phonon dispersion curves, crystal structures, density of states, Bader charges, and crystallographic lattice information.
- [51] A. Togo and I. Tanaka, *Scr. Mater.* **108**, 1 (2015).
- [52] P. Giannozzi, S. Baroni, N. Bonini, M. Calandra, R. Car, C. Cavazzoni, D. Ceresoli, G. L. Chiarotti, M. Cococcioni I. Dabo *et al.*, *J. Phys.: Condens. Matter* **21**, 395502 (2009).
- [53] P. B. Allen and R. C. Dynes, *Phys. Rev. B* **12**, 905 (1975).
- [54] Q. Chen, S. C. Bae, and S. Granick, *Nature (London)* **469**, 381 (2011).
- [55] R. Dronskowski and P. E. Bloechl, *J. Phys. Chem.* **97**, 8617 (1993).
- [56] V. L. Deringer, A. L. Tchougreff, and R. Dronskowski, *J. Phys. Chem. A* **115**, 5461 (2011).
- [57] S. Maintz, V. L. Deringer, A. L. Tchougreff, and R. Dronskowski, *J. Comput. Chem.* **37**, 1030 (2016).